Supplementary Figures (Fig. SI 1 to 12)

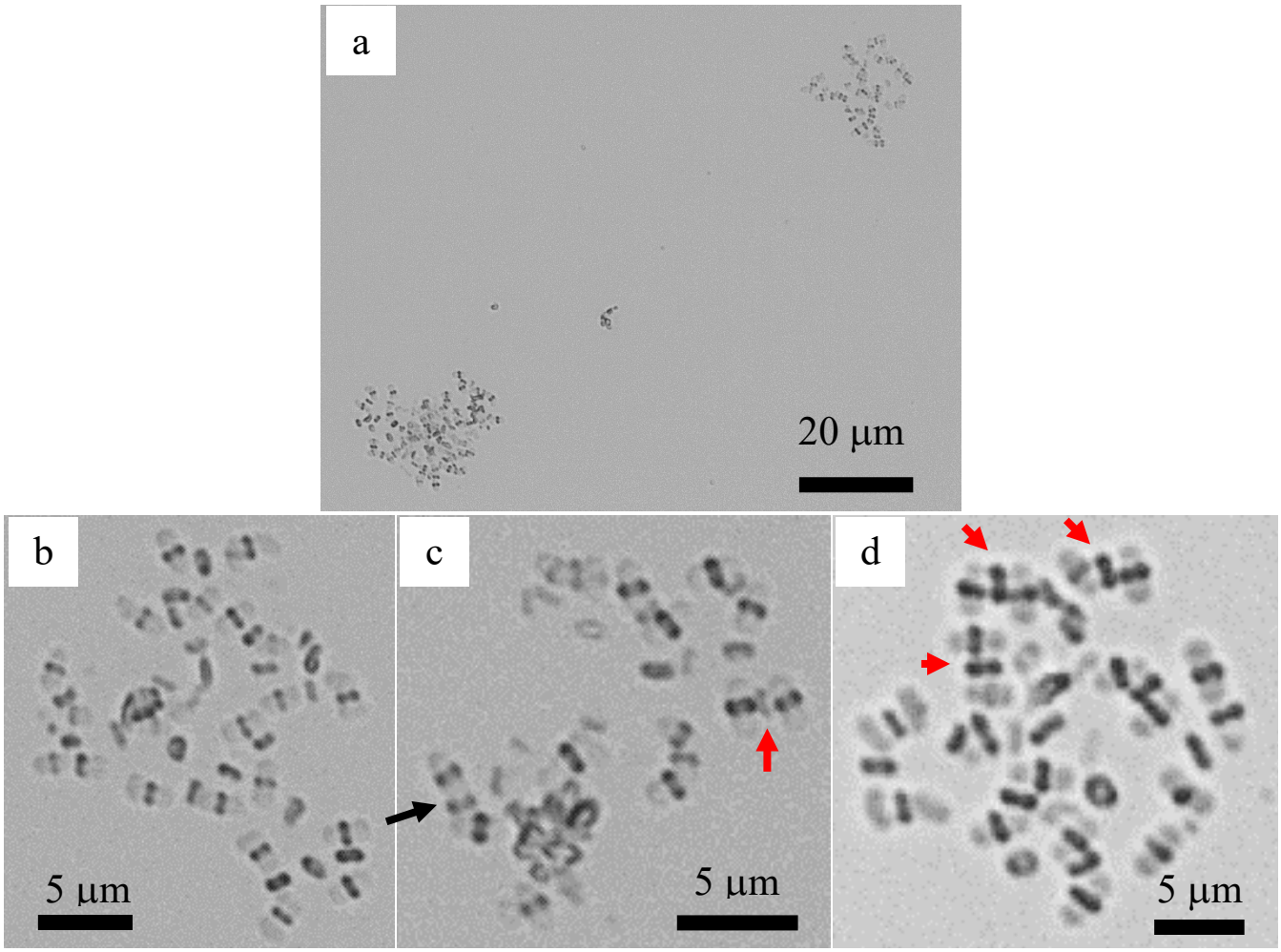

Supplementary Figure 1: Light microscopy of cyanobacterial cells forming (Fe, Mn)-rich silicate rings. Samples were collected in 2018 at a 2-meter depth. Red arrows show locations where two most recent rings formed by dividing cells are perpendicular to the ring that formed one division step ago. The black arrow shows one case where rings are in the same direction, possibly suggesting that consecutive division planes had the same direction.

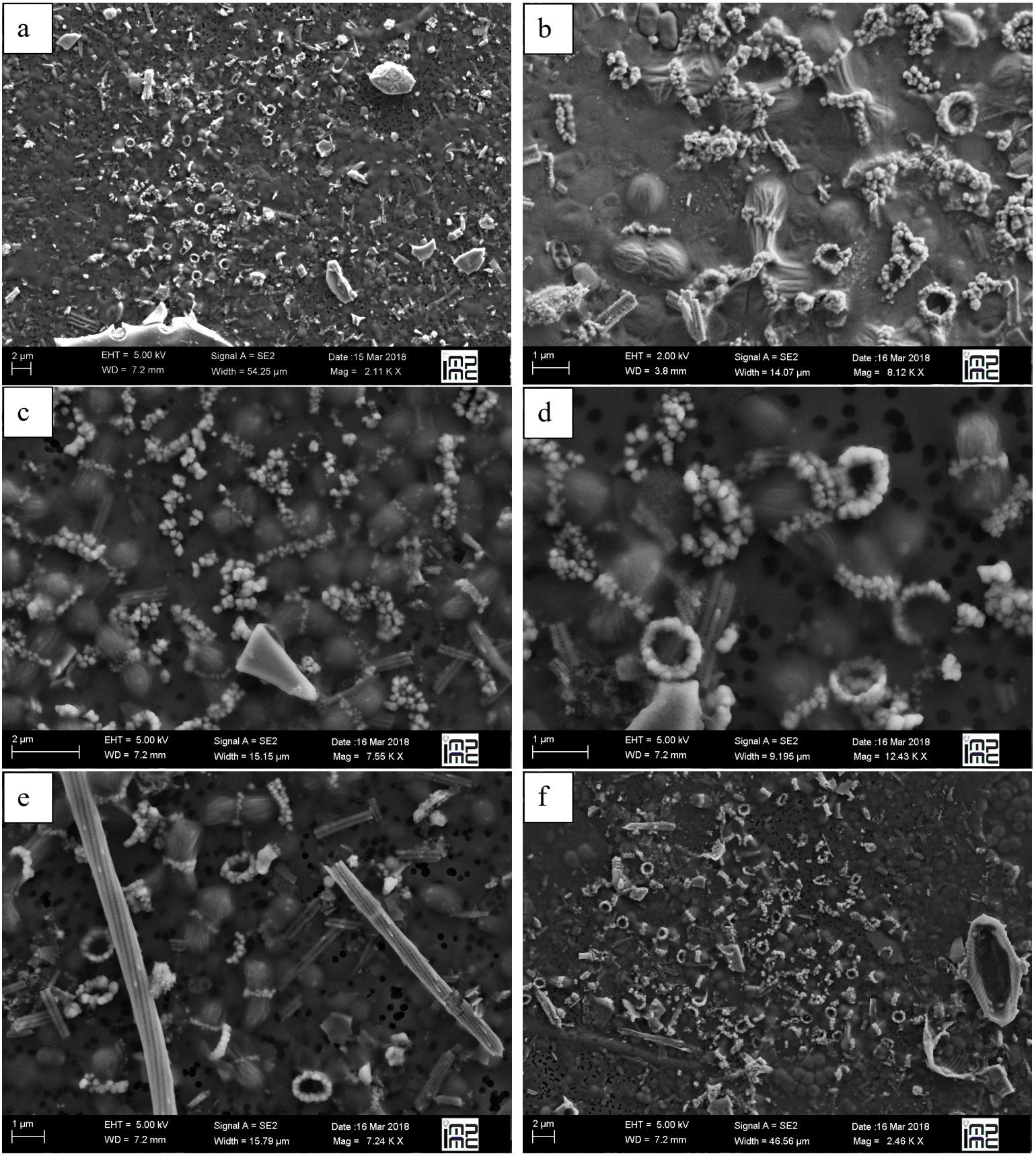
a
2 µm
EHT = 5.00 kV
WD = 7.2 mm
Signal A = SE2
Width = 54.25 µm
Date :15 Mar 2018
Mag = 2.11 K X
b
1 µm
EHT = 2.00 kV
WD = 3.8 mm
Signal A = SE2
Width = 14.07 µm
Date :16 Mar 2018
Mag = 8.12 K X
c
2 µm
EHT = 5.00 kV
WD = 7.2 mm
Signal A = SE2
Width = 15.15 µm
Date :16 Mar 2018
Mag = 7.55 K X
d
1 µm
EHT = 5.00 kV
WD = 7.2 mm
Signal A = SE2
Width = 9.195 µm
Date :16 Mar 2018
Mag = 12.43 K X
e
1 µm
EHT = 5.00 kV
WD = 7.2 mm
Signal A = SE2
Width = 15.79 µm
Date :16 Mar 2018
Mag = 7.24 K X
f
2 µm
EHT = 5.00 kV
WD = 7.2 mm
Signal A = SE2
Width = 46.56 µm
Date :16 Mar 2018
Mag = 2.46 K X

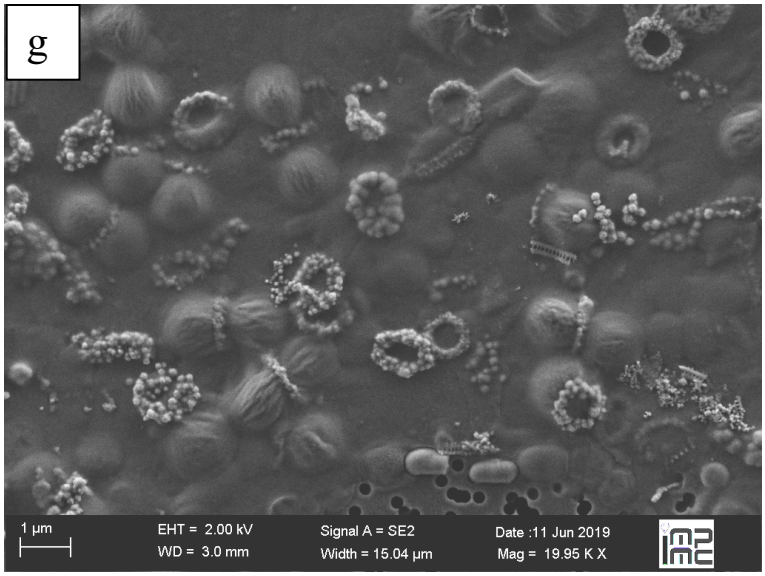
g
1 µm
EHT = 2.00 kV
WD = 3.0 mm
Signal A = SE2
Width = 15.04 µm
Date :11 Jun 2019
Mag = 19.95 K X

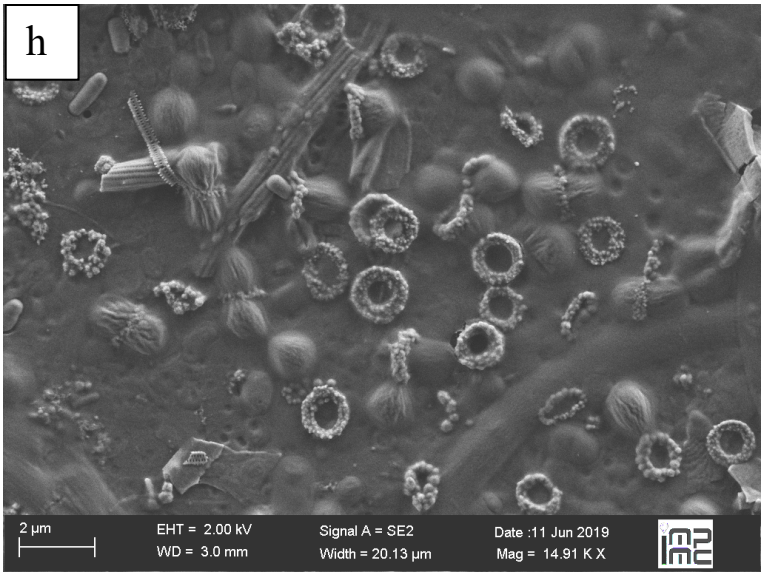
h
2 µm
EHT = 2.00 kV
WD = 3.0 mm
Signal A = SE2
Width = 20.13 µm
Date :11 Jun 2019
Mag = 14.91 K X

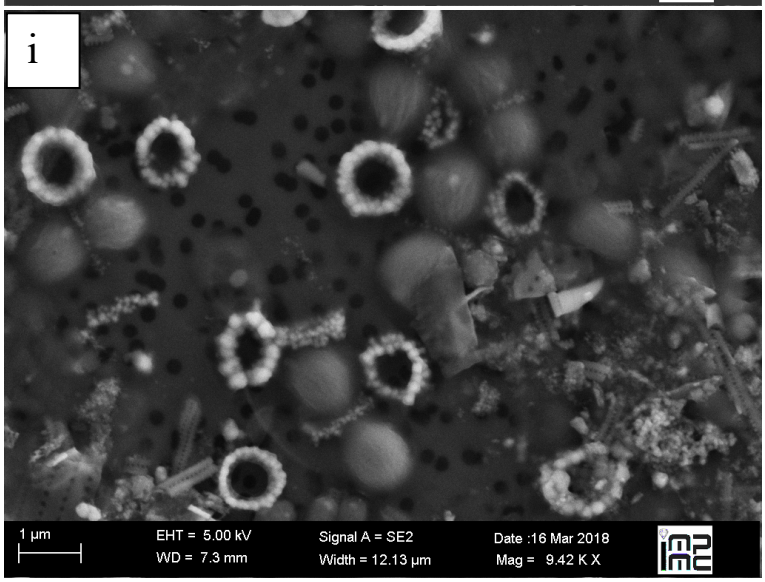
i
1 µm
EHT = 5.00 kV
WD = 7.3 mm
Signal A = SE2
Width = 12.13 µm
Date :16 Mar 2018
Mag = 9.42 K X

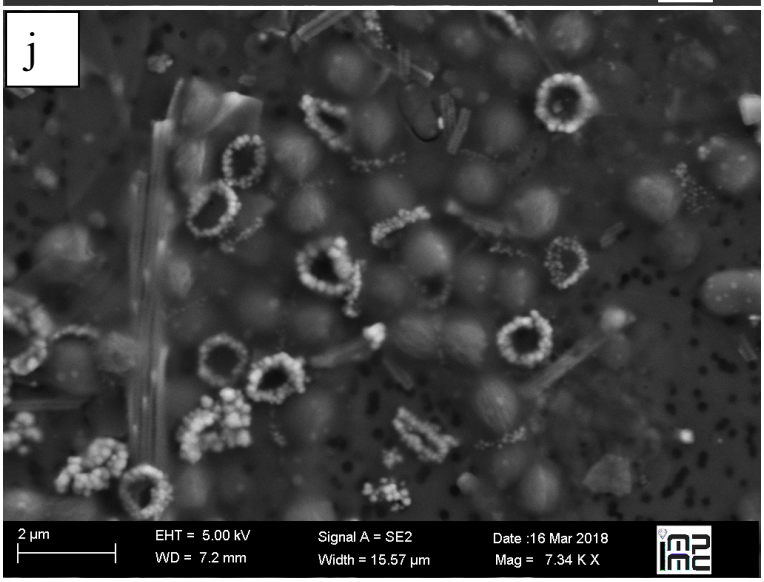
j
2 µm
EHT = 5.00 kV
WD = 7.2 mm
Signal A = SE2
Width = 15.57 µm
Date :16 Mar 2018
Mag = 7.34 K X

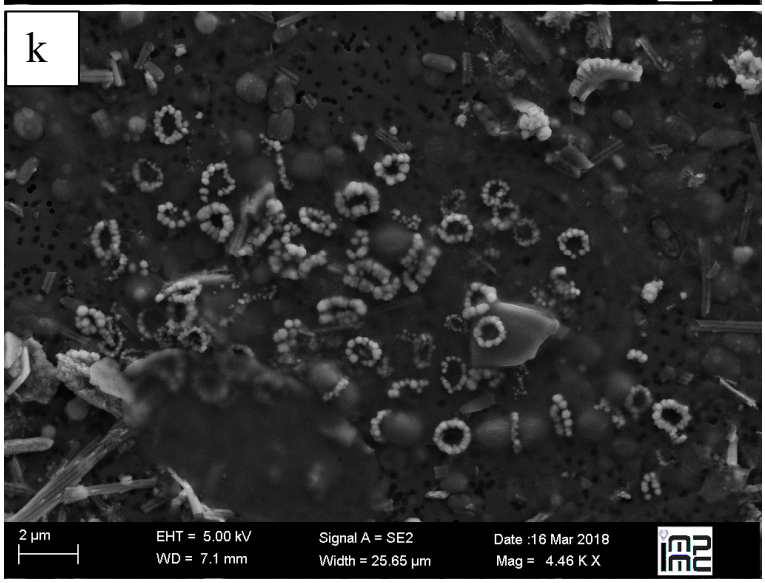
k
2 µm
EHT = 5.00 kV
WD = 7.1 mm
Signal A = SE2
Width = 25.65 µm
Date :16 Mar 2018
Mag = 4.46 K X

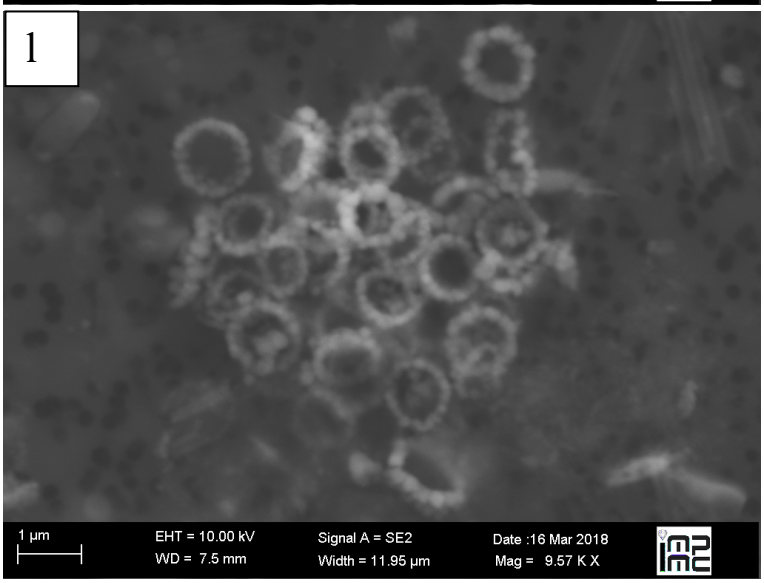
l
1 µm
EHT = 10.00 kV
WD = 7.5 mm
Signal A = SE2
Width = 11.95 µm
Date :16 Mar 2018
Mag = 9.57 K X

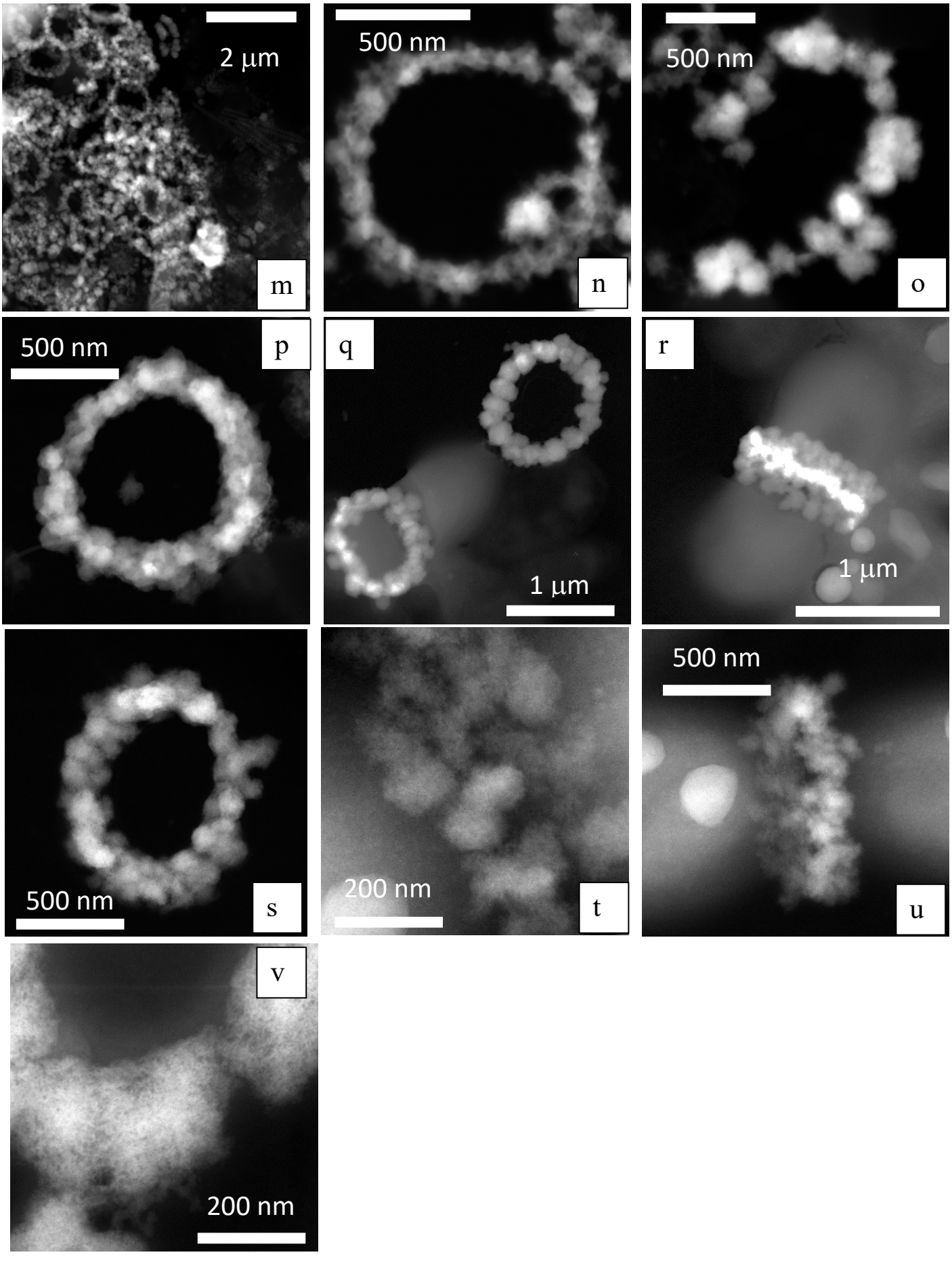
2 μm
m
500 nm
n
500 nm
o
500 nm
p
q
1 μm
r
1 μm
500 nm
s
200 nm
t
500 nm
u
v
200 nm

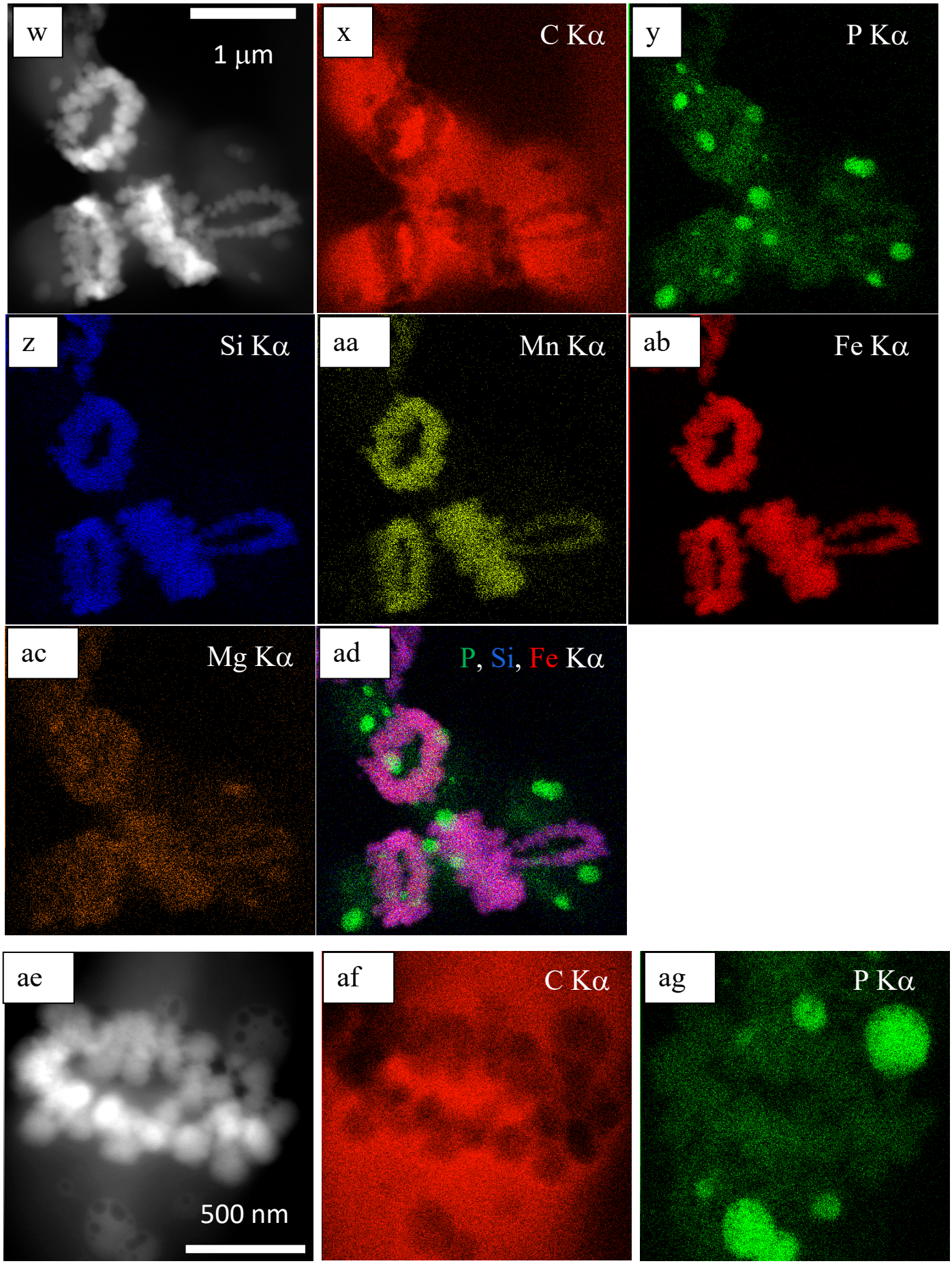
w
1 µm
x
C Kα
y
P Kα
z
Si Kα
aa
Mn Kα
ab
Fe Kα
ac
Mg Kα
ad
P, Si, Fe Kα
ae
500 nm
af
C Kα
ag
P Kα

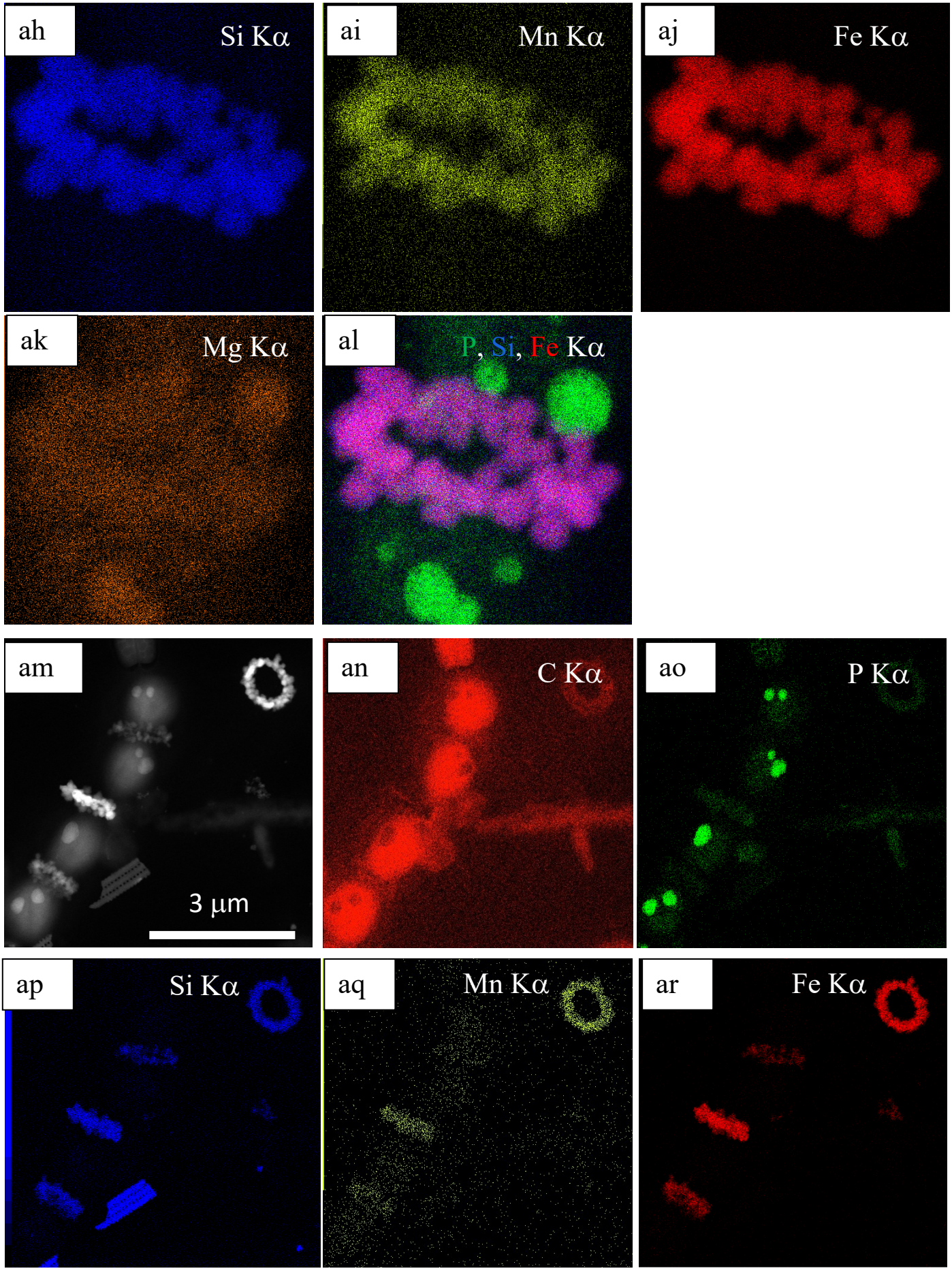
ah
Si Kα
ai
Mn Kα
aj
Fe Kα
ak
Mg Kα
al
P, Si, Fe Kα
am
3 µm
an
C Kα
ao
P Kα
ap
Si Kα
aq
Mn Kα
ar
Fe Kα

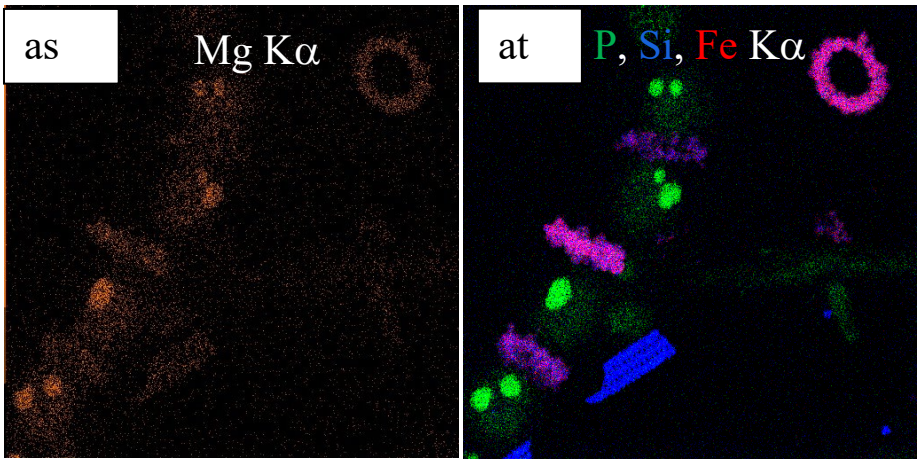

Supplementary Figure 2: Supplementary SEM, STEM and STEM-EDXS analyses. (a-b) SEM image of a sample collected in 2018 at 2 m; (C-F) SEM image of a sample collected in 2018 @ 10 m; (g-h)) SEM image of a sample collected in 2019 @ 15m; (i-j) SEM image of a sample collected in 2018 @18m; (k) SEM image of a sample collected in @25m (l) SEM image of a sample collected in @33 m; (m-r) STEM-HAADF image of rings collected in 2018 @ 39 m (s-v) STEM-HAADF image of rings collected in 2018 @ 4m. (w-ad): STEM-EDXS analyses of a cluster of cells collected in 2018 @ 4 m. (ae-al): STEM-EDXS analyses (STEM image and EDXS map) of a ring between two cells collected in 2018 @ 4 m. (am-at) STEM-EDXS analyses (AM is a STEM image and other images are chemical maps) of a cluster of cells collected in 2018 @ 4 m. All SEM images are obtained in the secondary electron detection mode.

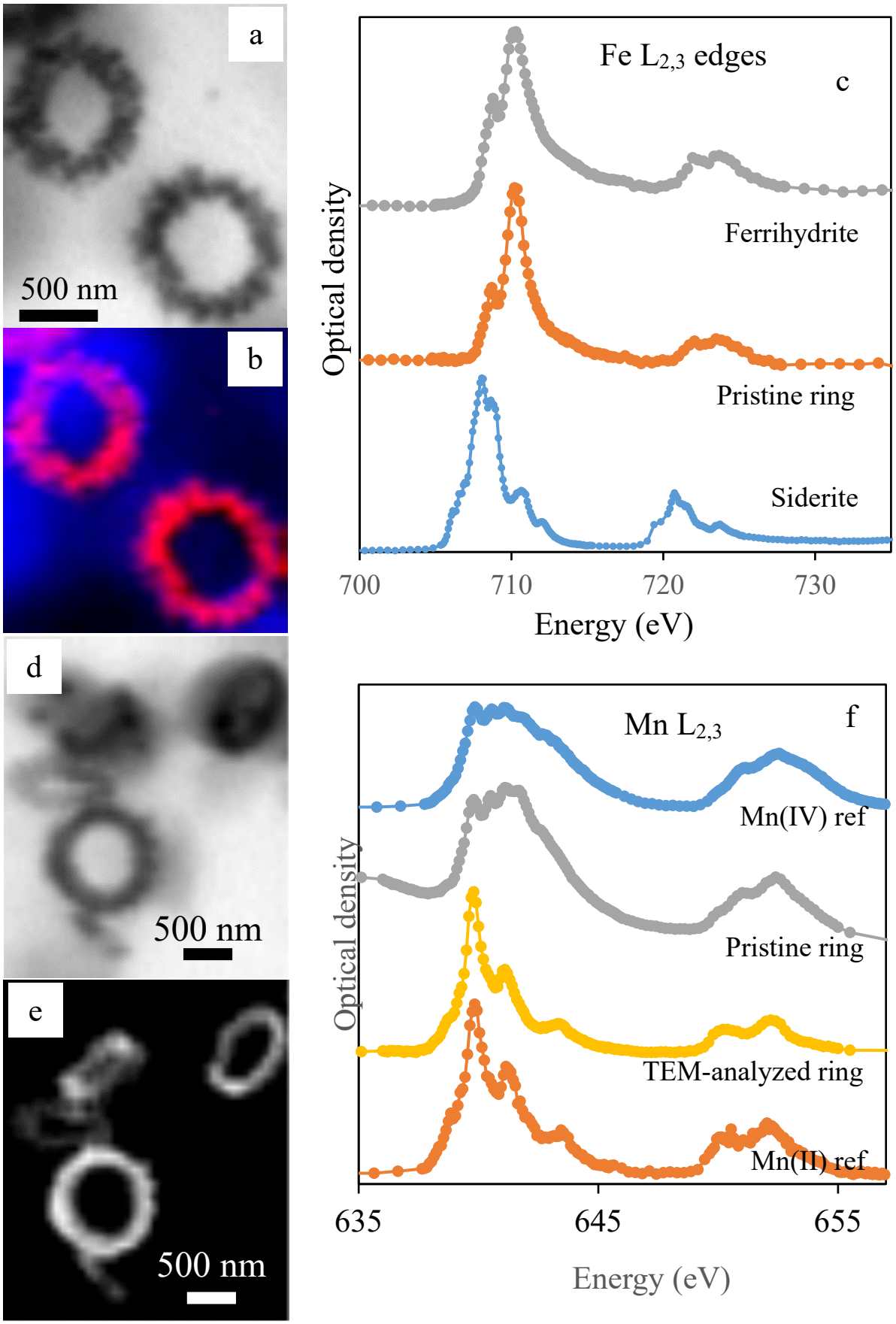
a
500 nm
b
d
500 nm
e
500 nm
Fe L2,3 edges
c
Ferrihydrite
Pristine ring
Siderite
Optical density
700
710
720
730
Energy (eV)
Mn L2,3
f
Mn(IV) ref
Pristine ring
TEM-analyzed ring
Mn(II) ref
Optical density
635
645
655
Energy (eV)

Supplementary Figure 3: (a-c): STXM analyses at the Fe $L_{2,3}$ edges. (a) STXM image at 710 eV of pristine rings (i.e. not irradiated by TEM before STXM analyses). (b) STXM map of Fe (in red); cells are shown in blue. (c) XANES spectrum at the Fe $L_{2,3}$ edge of reference ferrihydrite (Fe(III)), reference siderite (Fe(II)) and the La Preciosa silicate rings showing that Fe is mostly under the Fe(III) form in the rings. (d) image at 638 eV, at the Mn $L_{2,3}$ edges. (e) STXM map of Mn. (f) XANES spectra at the Mn $L_{2,3}$ edges of a Mn(II) [$HMnPO_4$) and Mn(IV) (birnessite) references as well as silicate rings irradiated by TEM beforehand or pristine during STXM analyses. Artefactual Mn reduction by the TEM beam can be detected in the spectrum

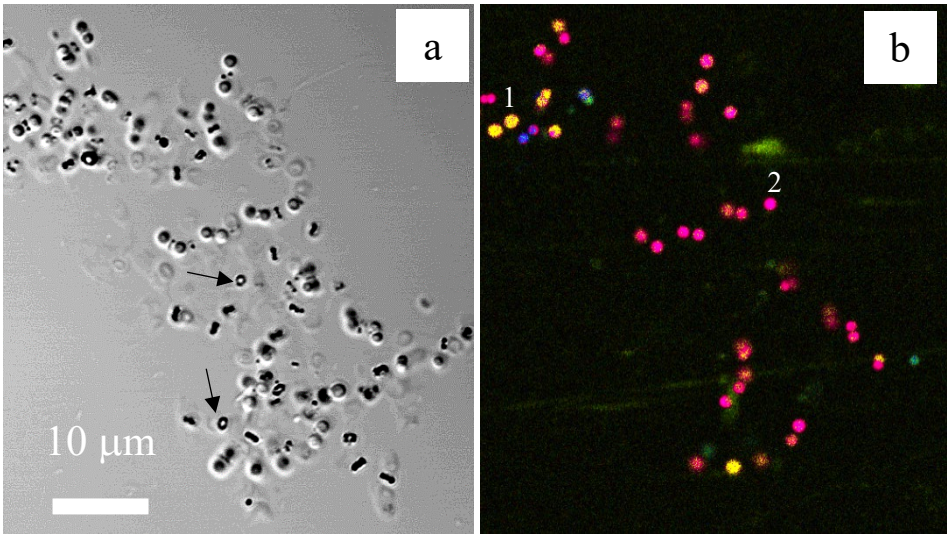
a
b
1
2
10 μm

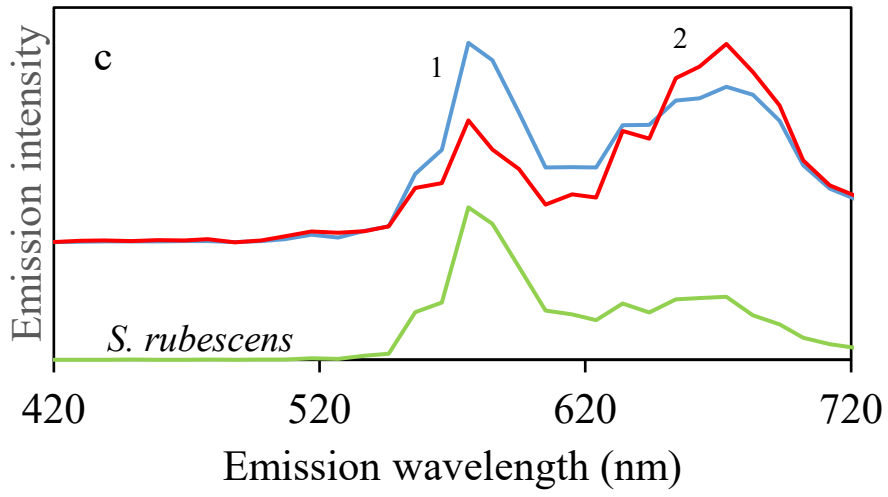
c
1
2
Emission intensity
S. rubescens
420
520
620
720
Emission wavelength (nm)

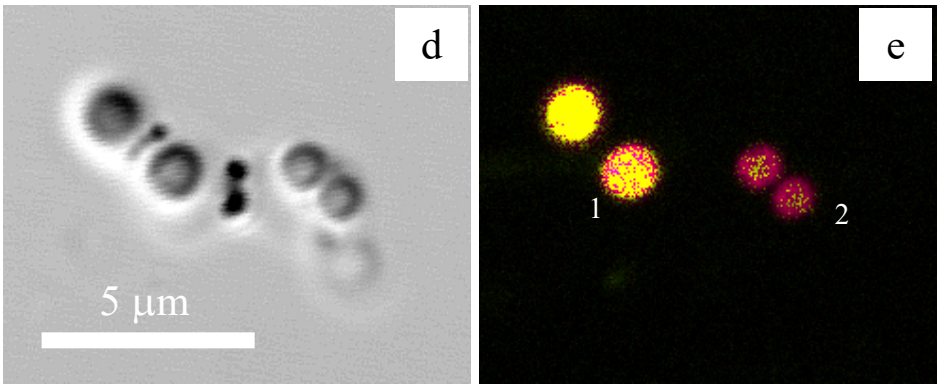
d
e
5 μm
1
2

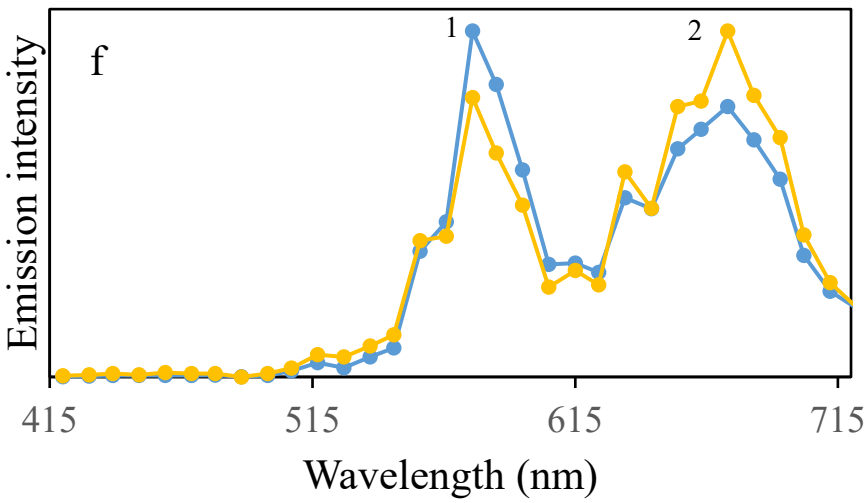
f
1
2
Emission intensity
415
515
615
715
Wavelength (nm)

Supplementary Figure 4: Confocal laser scanning microscopy analyses of bacteria forming (Fe, Mn)-rich silicate rings. (a) CLSM image of an aggregate of cells forming silicate rings in transmitted light detection. Some rings are viewed along their central axis (arrows). (b) Corresponding fluorescence emission image. False colours correspond to the colour of the emission light. Cells have varying colours corresponding in all cases to a mixture of yellow-orange (585 nm) and red (670 nm) in varying proportions. Excitation was performed at 405 and 488 nanometers. (c) Fluorescence emission spectra of two cells (noted 1 and 2 on b) together with a reference emission spectrum of the phycoerythrin-containing cyanobacterium *S. rubescens*. The main emission peaks are at 585 nm (phycoerythrin) and 670 nm (phycocyanin and chlorophyll). (d) CLSM image of two pairs of dividing cells forming silicate rings in transmitted light detection. (e) Corresponding fluorescence emission image. (f) Fluorescence emission spectra of two cells (noted 1 and 2 on e).

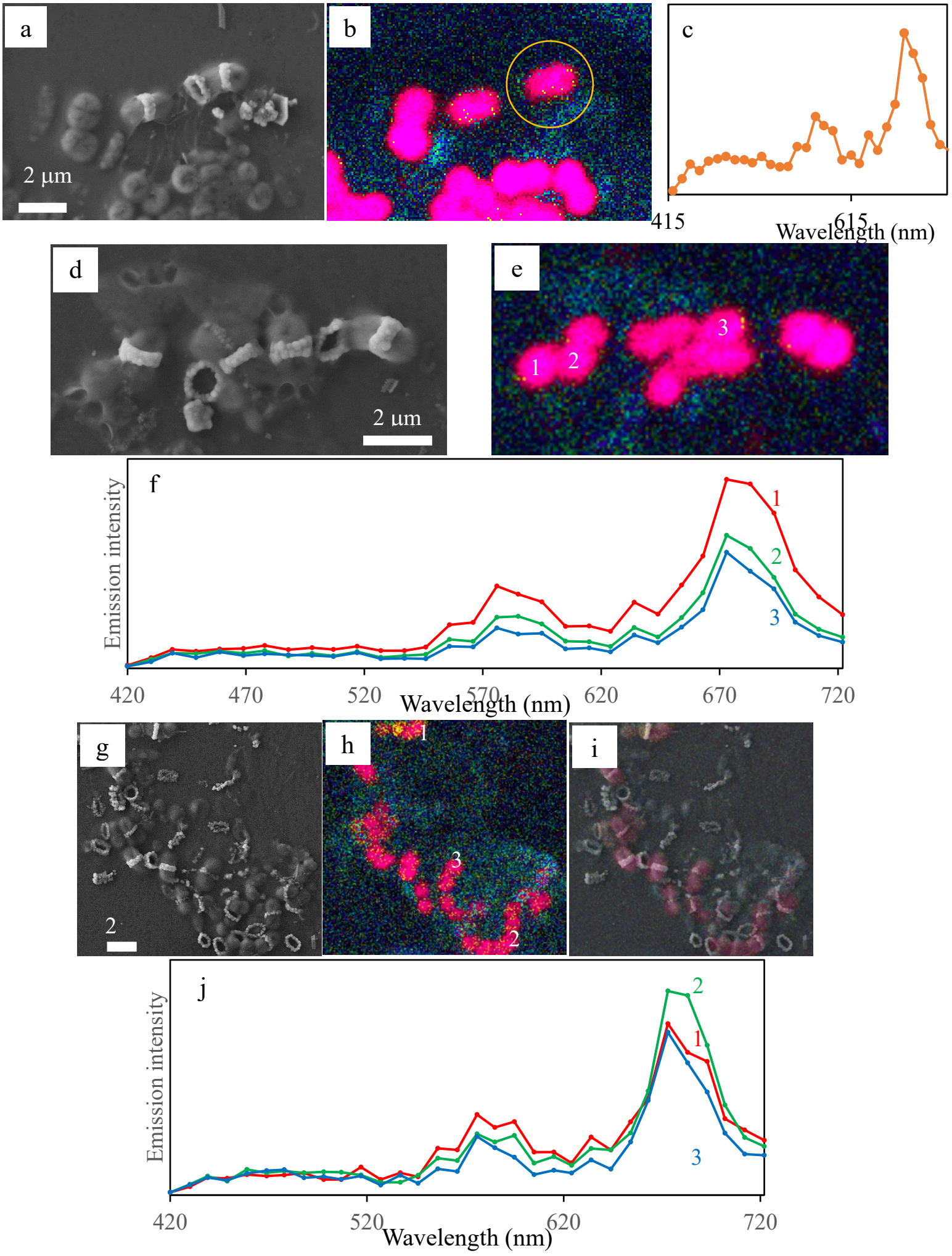
a
2 μm
b
c
415
615
Wavelength (nm)
d
2 μm
e
1
2
3
f
Emission intensity
1
2
3
420
470
520
570
620
670
720
Wavelength (nm)
g
2
h
1
3
2
i
j
Emission intensity
2
1
3
420
520
620
720
Wavelength (nm)

Supplementary Figure 5: CLSM-SEM correlative microscopy of bacteria forming (Fe, Mn)-rich silicate rings. (a) SEM image in the secondary electron mode showing microbial cells (in grey) with three bright silicate rings. (b) Fluorescence emission image of the same area. Most cells, including some without rings show autofluorescence. The circle outlines the cell from which a fluorescence spectrum was measured. (c) Fluorescence emission spectrum of the cell outlined in (b). (d) SEM image in the secondary electron mode showing several dividing cells forming silicate rings (bright). (e) Corresponding fluorescence emission image. Numbers refer to the spectra shown in (f). (f) Fluorescence emission spectra of three cells (noted 1-3 on e). (G) SEM image in the secondary electron mode showing several dividing cells forming silicate rings (bright). (h) Corresponding fluorescence emission image. Numbers refer to the spectra shown in (j). (i) Overlay of the SEM image and the fluorescence emission image (pink). (j) Fluorescence emission spectra of three cells (noted 1-3 on h). In all cases, excitation was performed at 405 nanometers only.

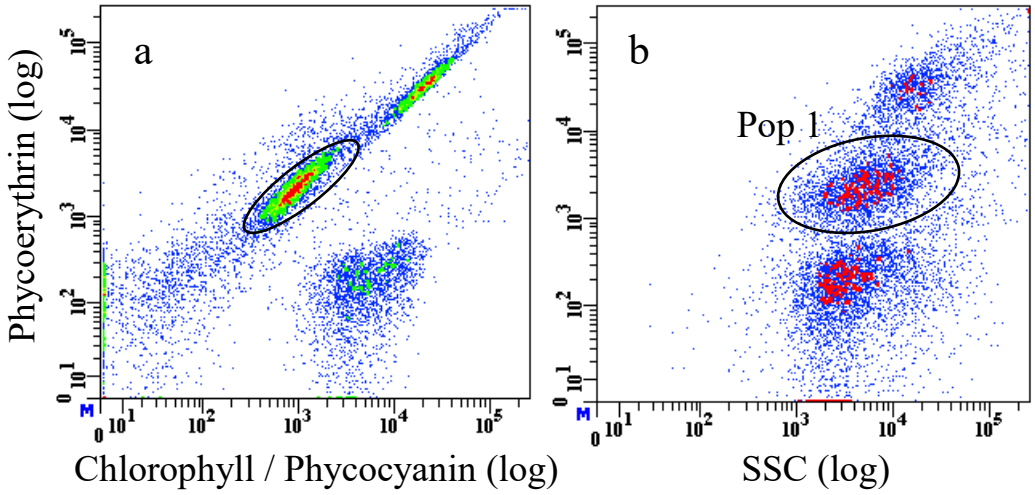
a
b
Pop 1
Phycoerythrin (log)
Chlorophyll / Phycocyanin (log)
SSC (log)

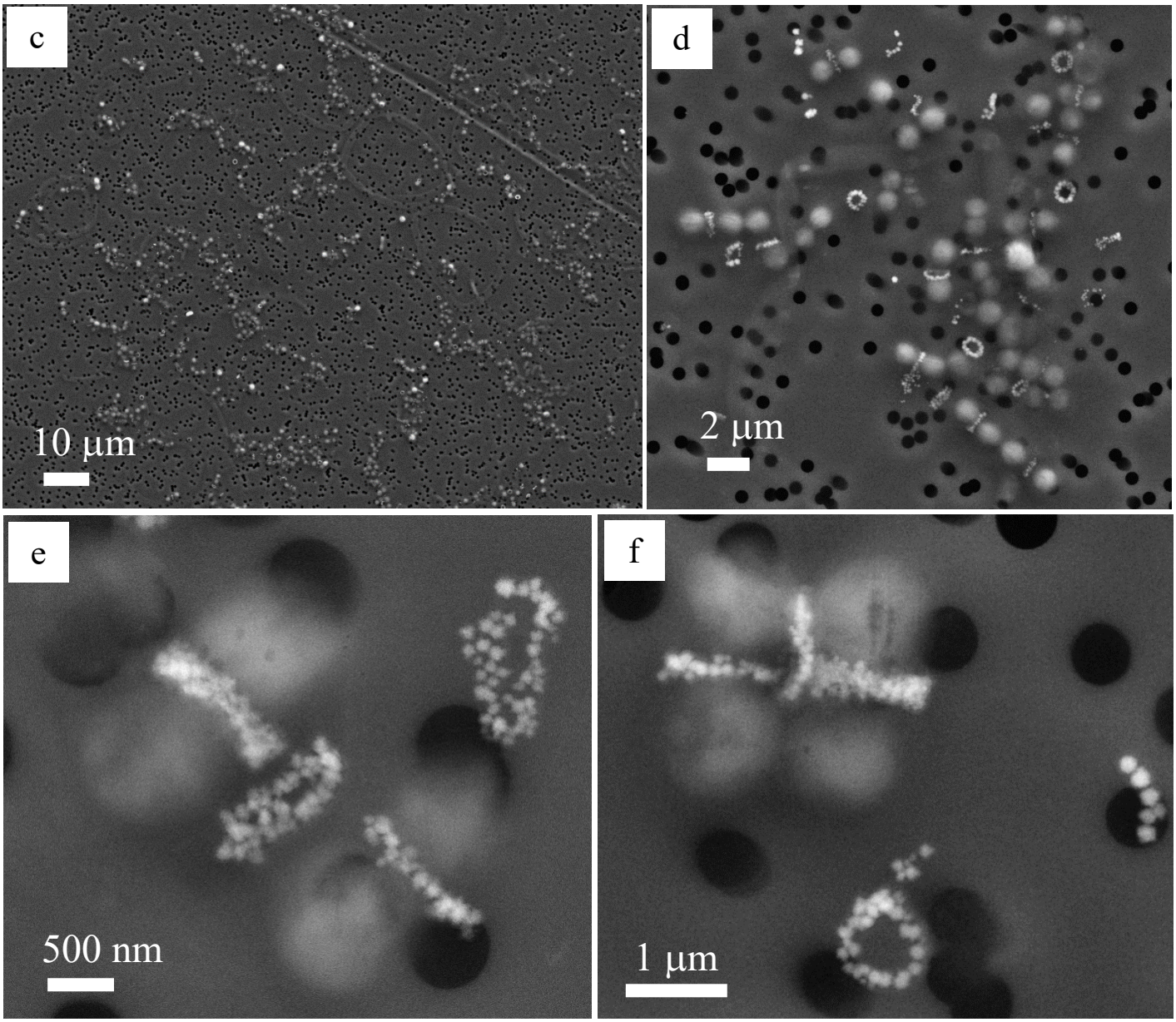
c
10 µm
d
2 µm
e
500 nm
f
1 µm

Supplementary Figure 6: Results of cell sorting by flow cytometry. (a-b) Density plot cytograms with sorted Pop 1 idicated in black. 10,000 events are showed. Colours were calculated with the "probability method", each color level represents 20% of the total events. (c-f) Scanning electron microscopy images of cells sorted by flow cytometry. Secondary electrons, 8 keV. (c) Low magnification image (field of view: 140 μm) showing mostly cells with silicate rings. d) Higher magnification view showing a cluster of ring-forming cells. e) Two couples of daughter cells separated by a perpendicular silicate ring, suggesting the existence of two perpendicular division planes. f) Same as e).

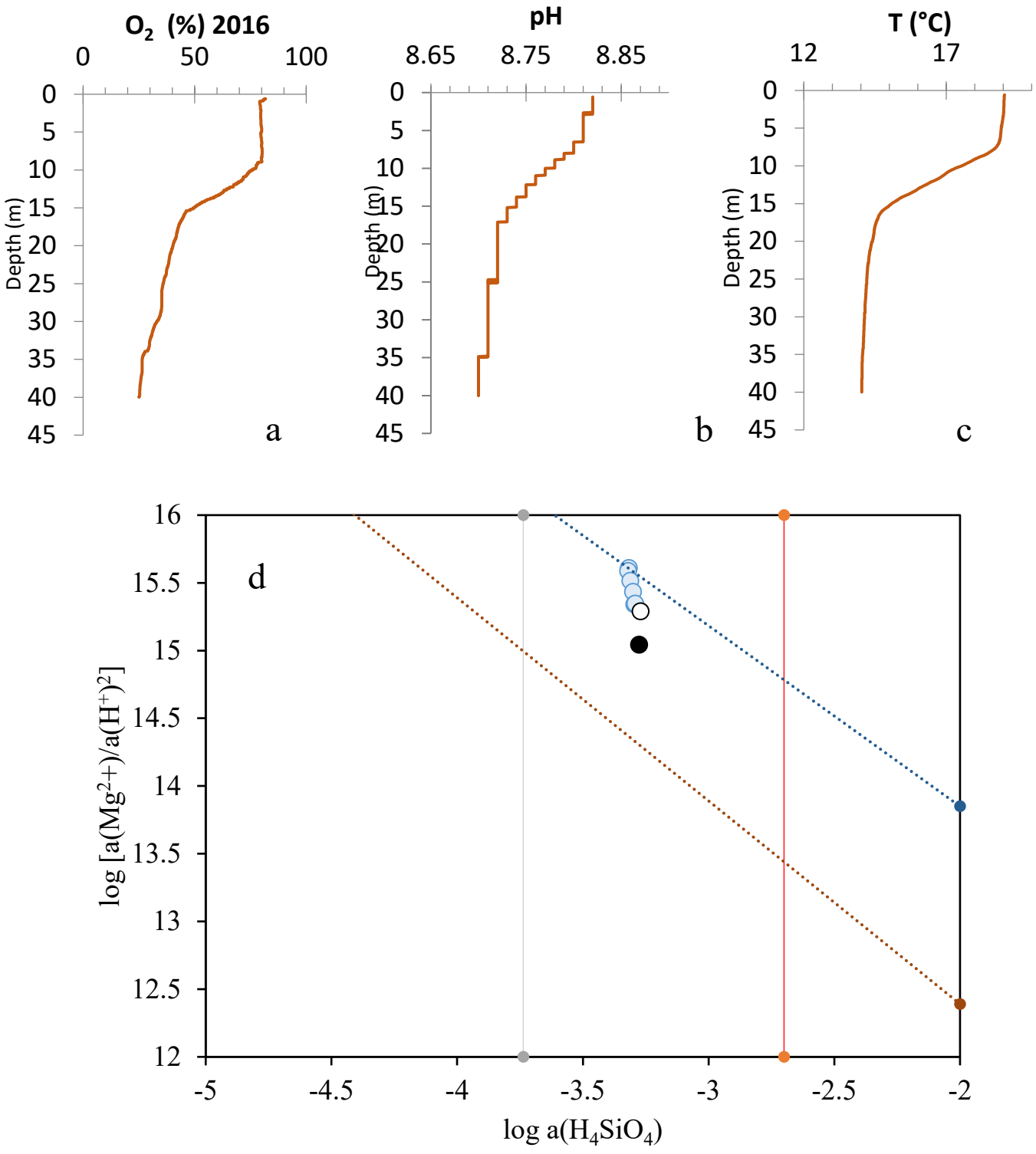

Supplementary Figure 7: (a) Depth profile of dissolved oxygen concentration in the water column of Lake La Preciosa in May 2016. (b) Depth profile of pH. (c) Depth profile of temperature. (d) Solubility diagram in the $\log[a(Mg^{2+})/a(H^{+})^2]$ – $\log[a(H_4SiO_4)]$ space

determined at 25 °C. La Preciosa surface water in January 2012 (cells were not observed by microscopy at this date; open circle), May 2014 (black filled circle) and water at different depth collected in May 2016 (blue circles) are plotted after correction of their temperature variations. The solubility line of the so-called amorphous sepiolite (Wollast et al., 1968), an amorphous Mg-silicate phase is indicated as a brown oblique line. Vertical dashed lines indicate the equilibrium solubility of quartz (grey) and amorphous silica (orange, Truesdell and Jones, 1974). The ‘‘critical saturation” line (blue oblique line) results from experiments conducted by Tosca et al., (2011) and Tosca and Masterson (2014) and relates to homogeneous nucleation of Mg-silicate phases from solution.

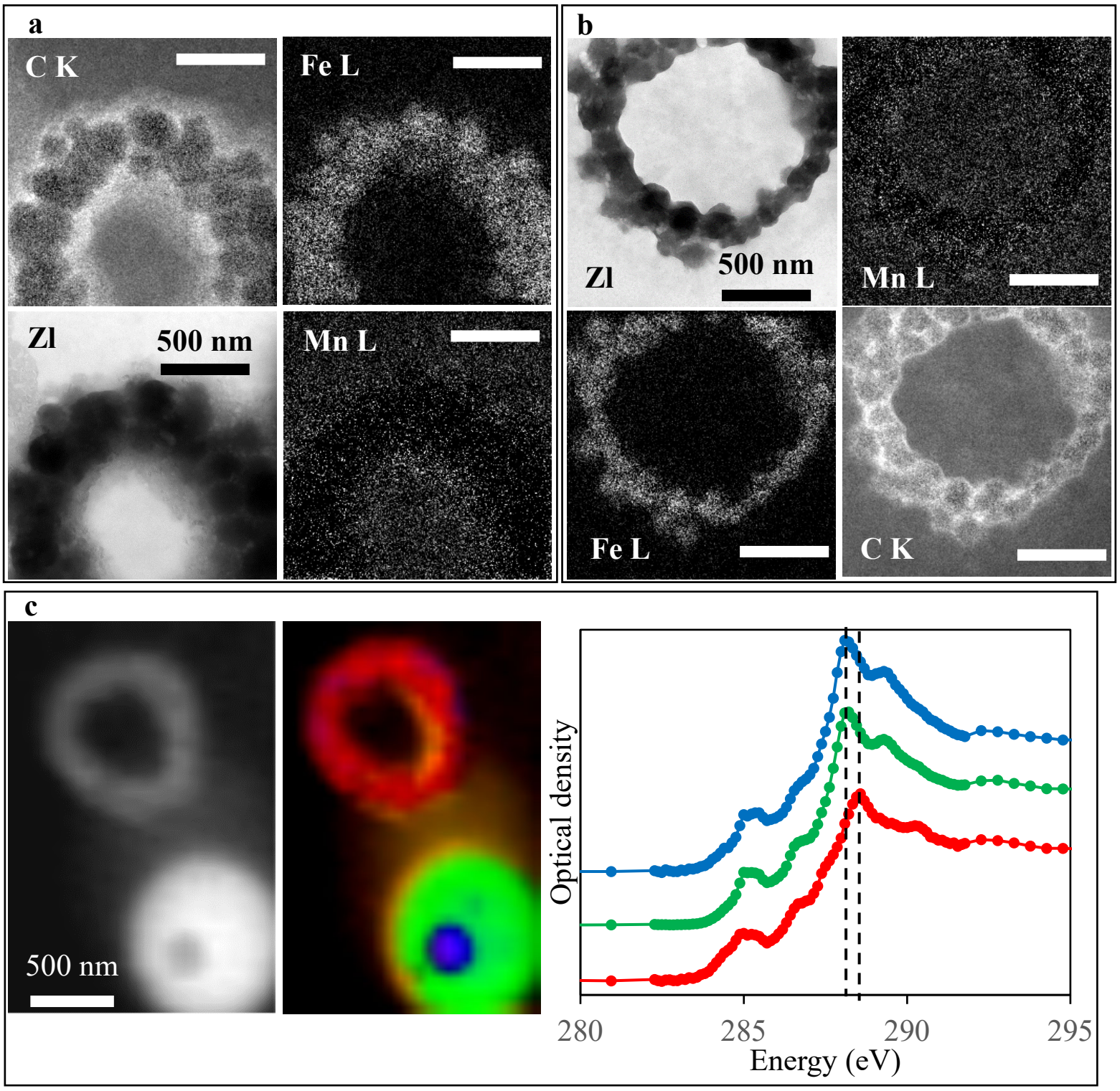

Supplementary Figure 8: Microscopy evidence of an organic envelope surrounding the silicate rings. (a) and (b): Energy-filtered transmission electron microscopy imaging of two different rings. C K: carbon map achieved based on the C K-edge; Fe L: Fe map based on the Fe $L_{2,3}$ edges. Mn L: Manganese map based on Mn $L_{2,3}$ edges; Zl: zero loss image using only elastically scattered electrons. (c) STXM analyses of one cell (bottom) and one silicate ring

(top). Left: carbon map achieved by subtracting an OD converted STXM image taken below the C K-edge (280 eV) from an OD-converted STXM image taken above the C K-edge (288.5 eV). Middle: map of three different carbon-containing compounds based on their different spectra at the C K-edge. Based on the XANES spectra and TEM observations: in blue: a polyphosphate inclusion; in green a cell; in red: a ring and extrapolymeric substance surrounding the cell. Right: XANES spectra at the C K-edge of the three compounds mapped in the middle image with corresponding colour code. The two dashed lines at 288.2 and 288.6 eV are interpreted as $1s \rightarrow \pi^*$ electron transition in C of amide and carboxylic groups, respectively (Benzerara et al., 2005).

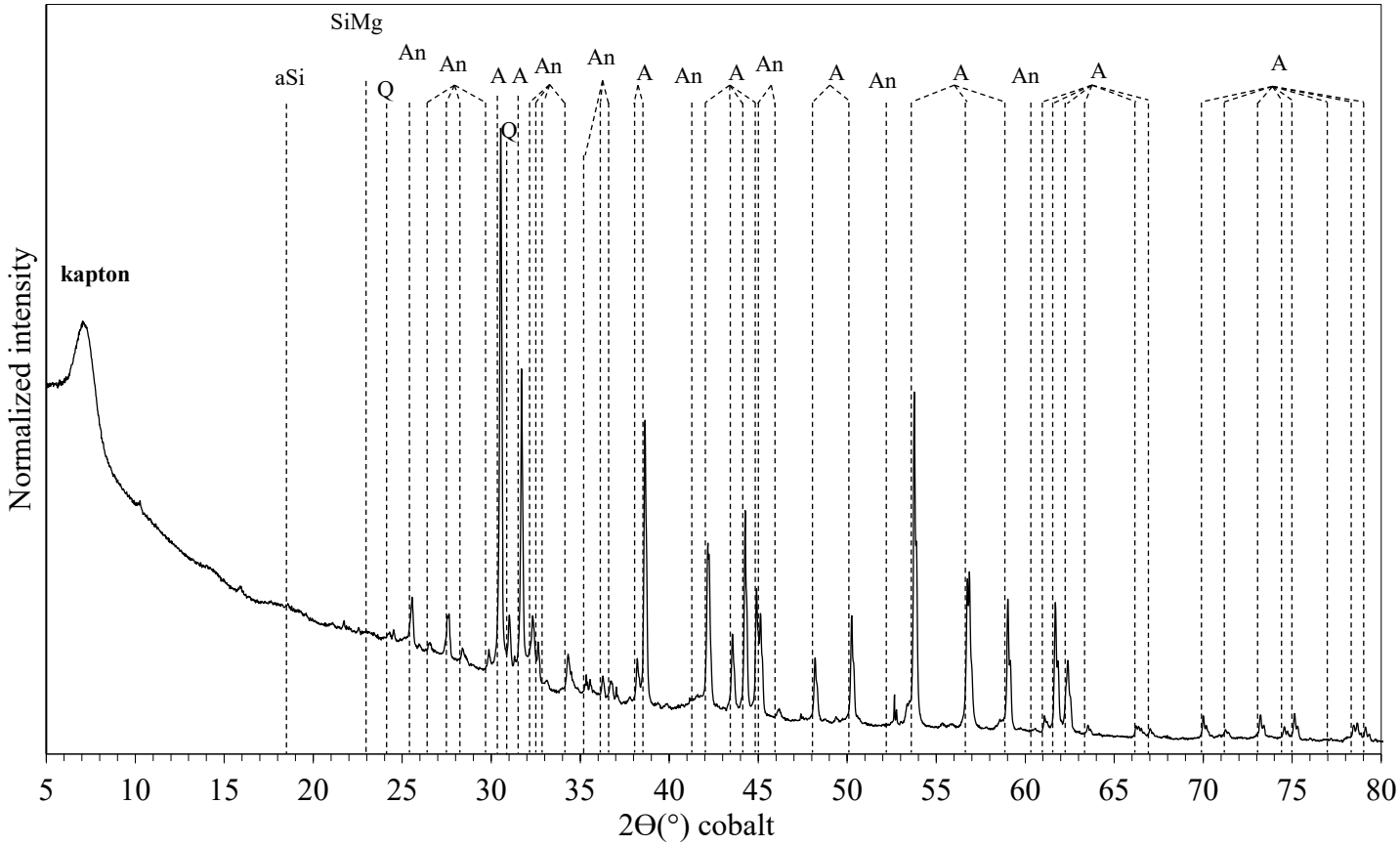
SiMg
aSi
An
An
Q
A A
An
An
A
An
A
An
A
An
A
An
A
An
A
A
Q
kapton
Normalized intensity
5
10
15
20
25
30
35
40
45
50
55
60
65
70
75
80
2Θ(°) cobalt

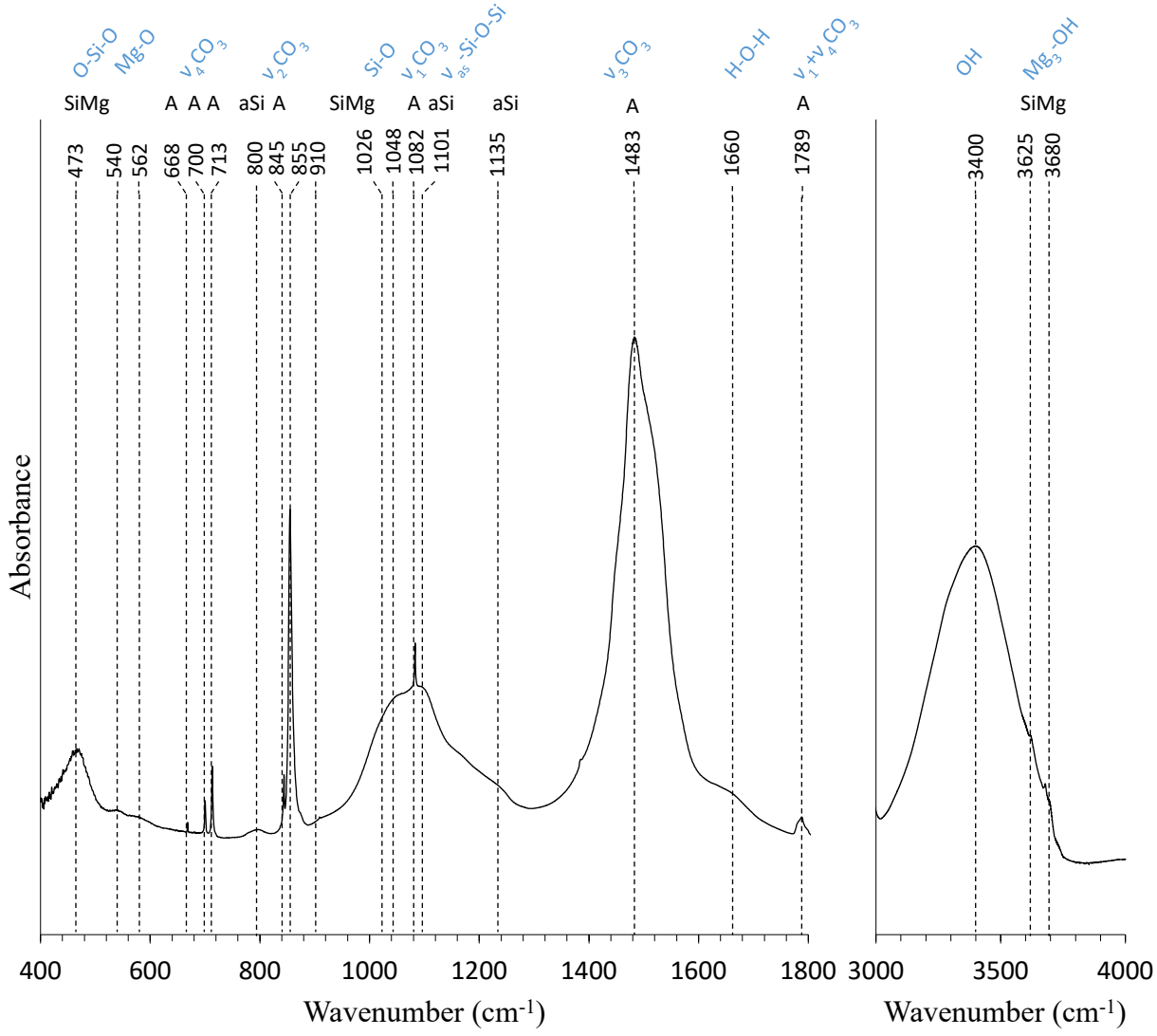
O-Si-O
Mg-O
ν4CO3
ν2CO3
Si-O
ν1CO3
νas-Si-O-Si
ν3CO3
H-O-H
ν1+ν4CO3
OH
Mg3-OH
SiMg
A A A
aSi A
SiMg
A aSi
aSi
A
A
SiMg
473
540
562
668
700
713
800
845
855
910
1026
1048
1082
1101
1135
1483
1660
1789
3400
3625
3680
Absorbance
400
600
800
1000
1200
1400
1600
1800
Wavenumber (cm-1)
3000
3500
4000
Wavenumber (cm-1)

Supplementary Figure 9: Top: x-ray diffraction patterns of La Preciosa sediments sampled at 1 cm depth. aSi: amorphous silica; SiMg: hydrated magnesium silicate (kerolite or stevensite); Q: quartz: An: plagioclase; A: aragonite. Mg-silicates are hardly visible by XRD. Bottom: Fourier transform infrared (FTIR) spectrum of the same sediment sample.

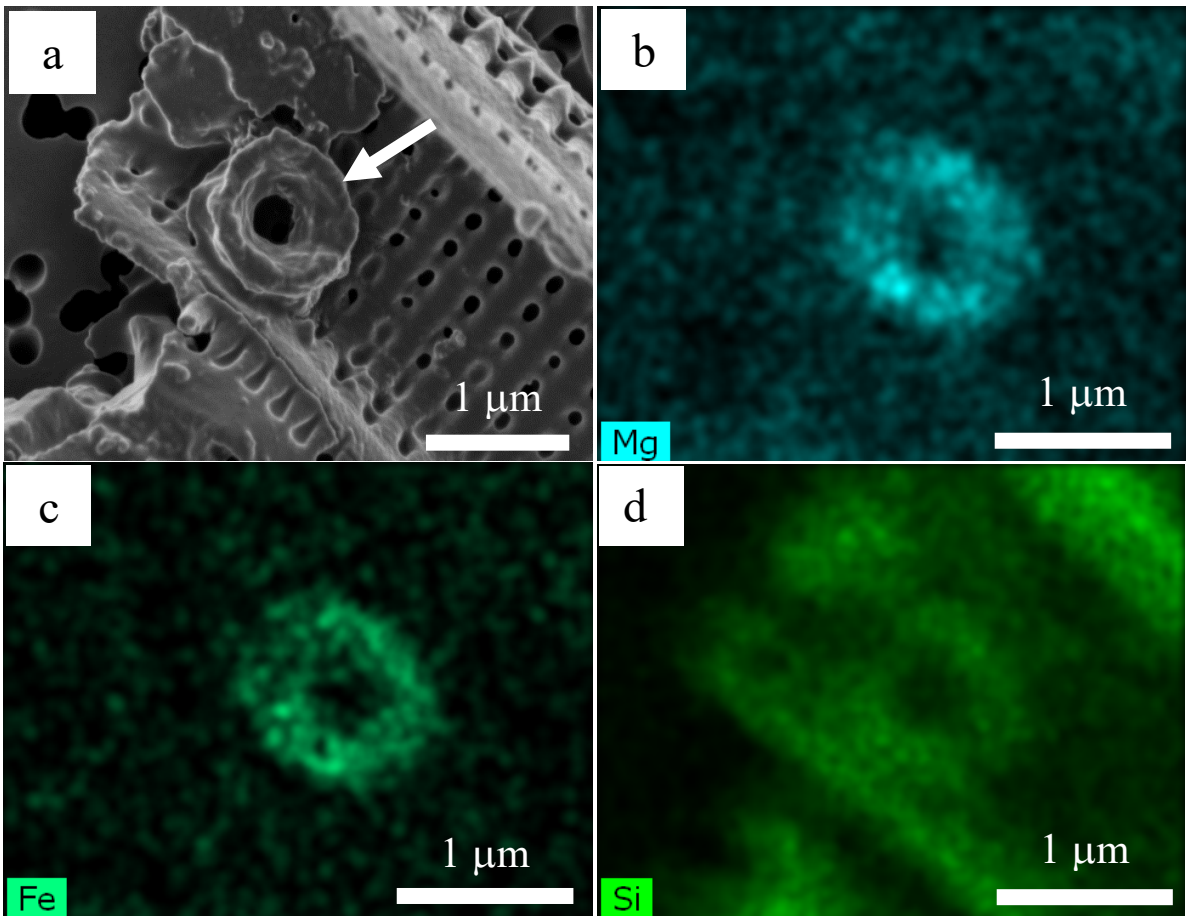
a
1 μm
b
Mg
1 μm
c
Fe
1 μm
d
Si
1 μm
e
1 μm
f
Si
1 μm
g
Mg
1 μm
h
Fe
1 μm

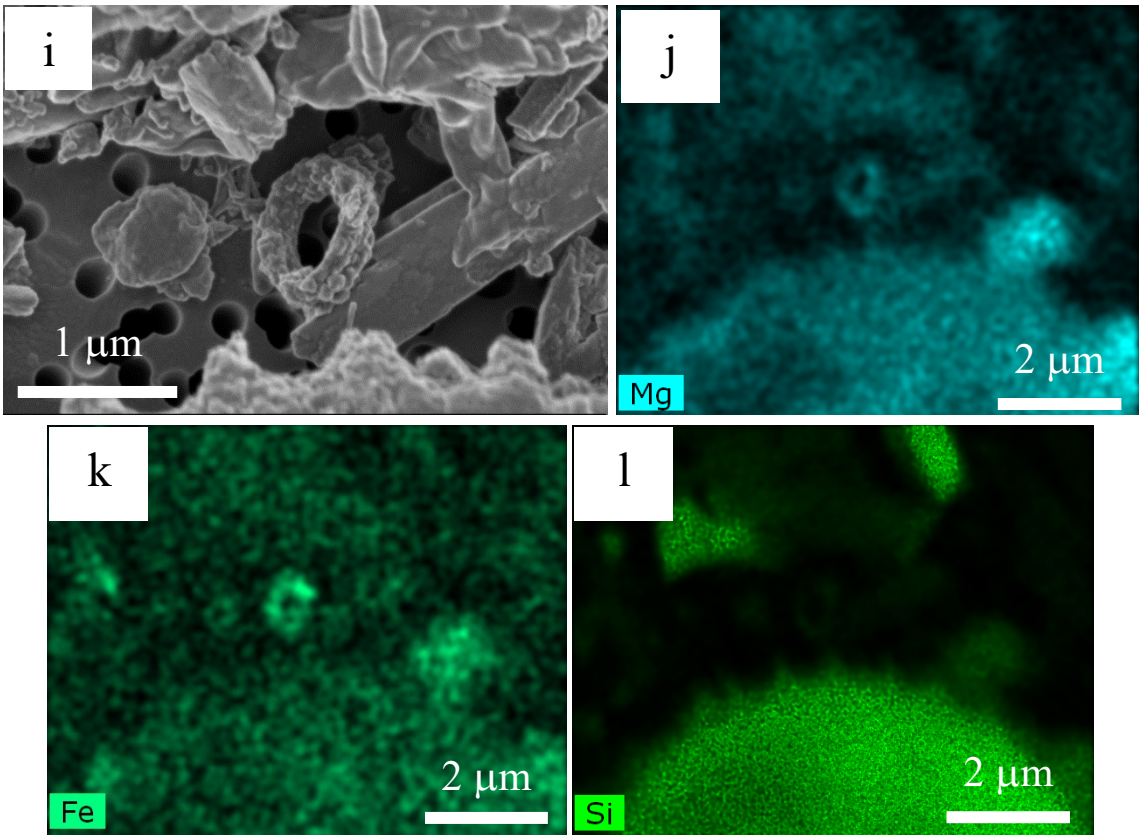

Supplementary Figure 10: SEM analyses of (Fe,Mn)-silicate rings in Lake La Preciosa sediments. These samples were pristine and not acid leached. (a-d) SEM image obtained in the secondary electron detection mode and chemical maps of Mg, Fe and Si of sediments sampled in 2016 at 9 cm in depth in the core. (e-h) Sediments also sampled in 2016 at a 9 cm depth in the sediment core. (i-l) Sediments sampled in 2016 at a 3 cm depth in the sediment core. Note in a and e (arrows) that the surface of the rings seems to be covered by a smooth and folded layer, suggesting that they are covered by organics.

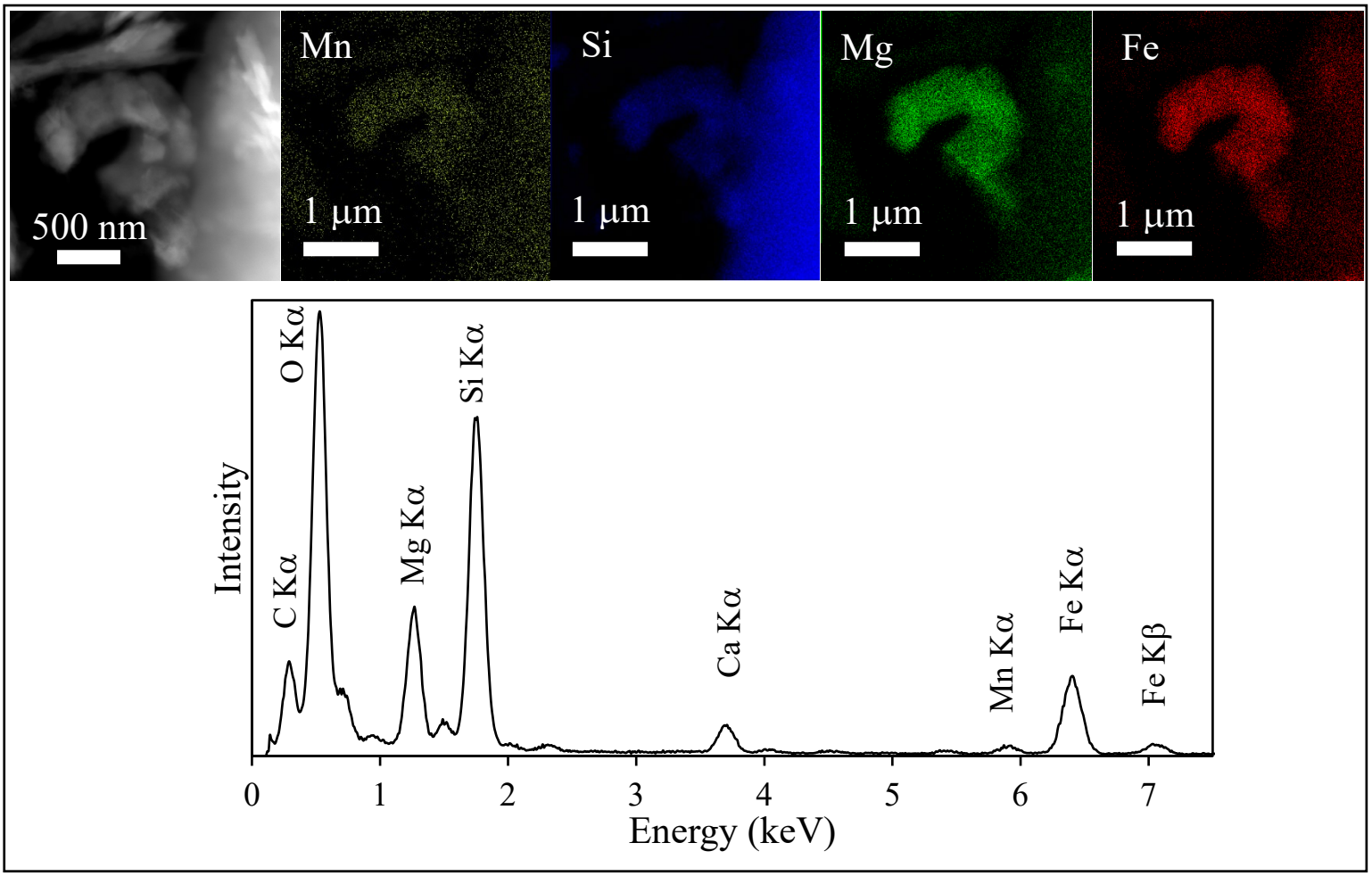

Supplementary Figure 11: STEM-EDXS analyses of silicate rings in sediments. STEM image, EDXS chemical maps of Mn, Si, Mg and Fe. Corresponding EDXS spectra of the rings showing the presence of Mg, Si and Fe as major elements. Some Ca is also detected. Sediment was acetic-acid-leached to concentrate rings in the TEM sample. Sediments were sampled in 2016 at 1 cm in depth in the sediment core. The same ring was analysed by STXM (see figure 4).

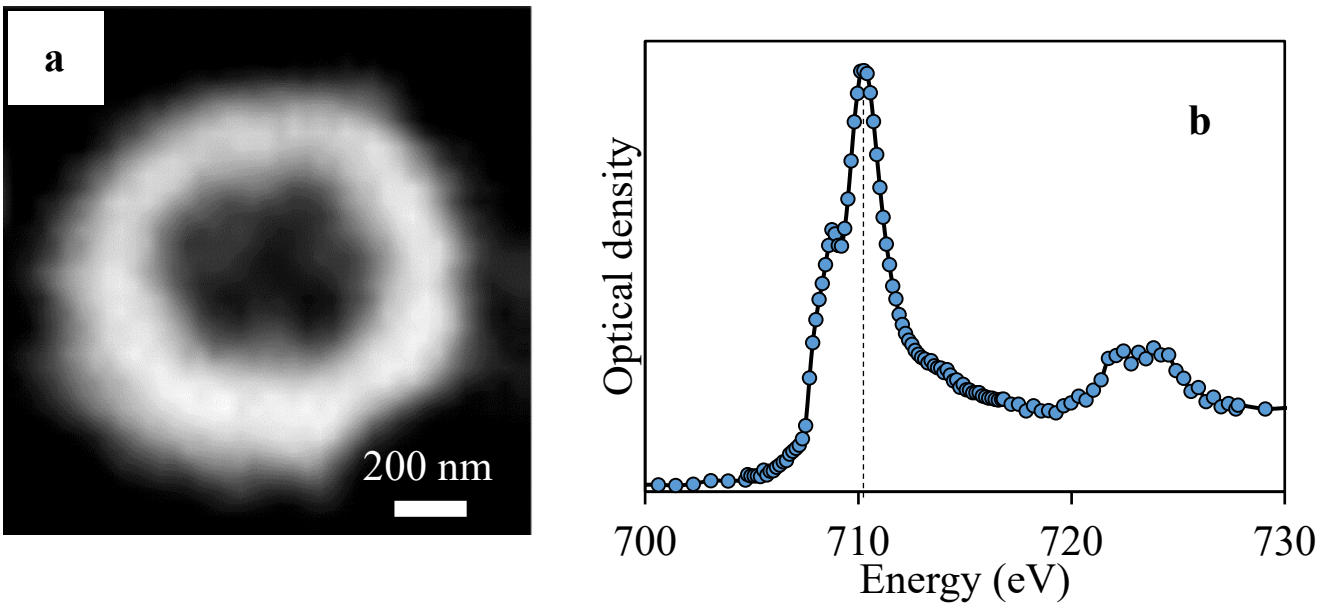

Supplementary Figure 12: STXM analyses of a (Fe,Mn)-rich silicate ring in the sediments at the Fe $L_{2,3}$ edges. a) Fe STXM map (@710-700 eV) after acid leaching of the carbonates. b) Corresponding XANES spectrum at the Fe $L_{2,3}$ edges. Dashed line is at 710.3 eV.